Aqueous Synthesis of Color-Tunable CuInS$_2$/ZnS Nanocrystals for the Detection of Human Interleukin 6

Wei-Wei Xiong, Guo-Hai Yang, Xing-Cai Wu,* and Jun-Jie Zhu*

State Key Lab of Analytical Chemistry for Life Science, Key Lab of Mesoscopic Chemistry of the MOE, and School of Chemistry and Chemical Engineering, Nanjing University, Nanjing 210093, P. R. China

S Supporting Information

ABSTRACT: In this Article, we present a facile microwave-assisted synthesis route for the preparation of water-soluble and high-quality CuInS$_2$/ZnS nanocrystals (NCs) with glutathione as the stabilizer. The as-prepared CuInS$_2$/ZnS NCs exhibited small particle sizes (~3.3 nm), long photoluminescence lifetimes, and color-tunable properties ranging from the visible to the near-infrared by varying the initial ratio of Cu/In in the precursors. The low-toxicity, highly luminescent and biocompatible CuInS$_2$/ZnS NCs were applied to cell imaging, showing that they could be used as promising fluorescent probes. Furthermore, the CuInS$_2$/ZnS NCs were used as the signal labels for a fluoroimmunoassay of the biomarker IL-6, showing their great potential for use as reliable point-of-care diagnostics for biomarkers of cancer and other diseases.

KEYWORDS: CuInS$_2$/ZnS nanocrystals, microwave assisted, color tunable, human interleukin-6, fluoroimmunoassay
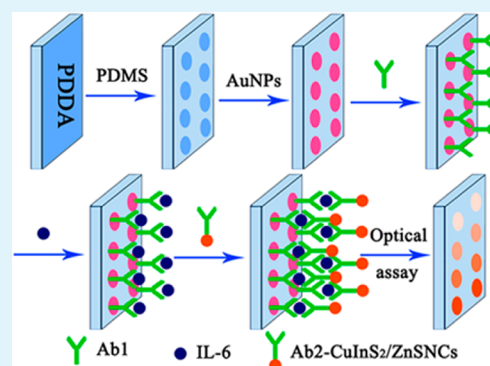
INTRODUCTION

In recent years, many researchers have devoted a lot of effort to the synthesis of near-infrared (NIR) fluorescence quantum dots (QDs) with long photoluminescence (PL) lifetimes, good biocompatibility, and small size particles (<5.5 nm) for biolabeling and bioimaging.[1−4] NIR fluorescence facilitates bioimaging and biodetection because it involves less autofluorescence interference and high transparency of biological tissues. Long photoluminescence lifetimes also decrease the autofluorescence background by using time-gated detection.[5] In recent years, syntheses of some NIR QDs have been reported, such as CdTeSe, CdTeSe/CdS, InAs, PbS, and so forth.[6−9] However, the applications of these NIR QDs have been hampered by their relatively high toxicity. Additionally, a small size is also important for labeling nanomaterials. In general, the sizes of most nanoparticles preclude their efficient clearance from the body. Without such clearance or their biodegradation into biologically benign components, toxicity is potentially amplified, and radiological bioimaging is hindered. A small size (<5.5 nm) can promote the rapid and efficient urinary excretion and elimination of QDs from the body.[4] Thus, it is extremely challenging to synthesize small-sized and low-toxicity NIR QDs.

CuInS$_2$ nanocrystals (NCs) have a low toxicity, long PL lifetime, and color-tunable properties ranging from the visible to the near-infrared.[5,10] They are considered to be alternative low-toxicity materials for biolabeling and bioimaging. Several methods have been reported for the synthesis of CuInS$_2$/ZnS NCs,[10−12] but they were carried out mostly in organic solvents, which may greatly limit their applications in life sciences because of their hydrophobicity. Very recently, some efforts have been devoted to the aqueous synthesis of CuInS$_2$ NCs, but they are limited by either low quantum yields or long production times.[13,14] Therefore, it is of great importance to develop a facile, rapid, aqueous synthesis route for high-quality CuInS$_2$/ZnS NCs. Microwave irradiation, which has rapid and uniform heating characteristics, is an attractive method for the synthesis of nanoparticles.[15] In comparison to conventional thermal techniques, microwave irradiation heating has two predominant merits: the temperature can be rapidly raised because of the high utilization factor of microwave energy, increasing the reaction rate by 1 to 2 orders of magnitude, and thermal gradient effects can be effectively reduced because of the volumetric heating of microwaves, which is favorable for realizing homogeneous heating, producing more uniform product formation.[16] Our research group succeeded in the preparation of quantum dots in an aqueous phase by the microwave-assisted methods described in previous reports.[17,18] A simple, rapid, and efficient synthesis route to water-soluble CuInS$_2$/ZnS NCs would be advantageous for the further development of their uses in biological and biomedical imaging.

Although CuInS$_2$/ZnS NCs have the advantages of low toxicity, high fluorescence, and long PL lifetimes, they are rarely applied in biological fields except for their use in imaging cells. The optical sensing use of CuInS$_2$/ZnS NCs is only in its infancy stage but has proven to be very promising.[5,13,19] Fluoroimmunoassays (FIA), which are based on selective antigen−antibody

binding and a fluorescence label, have gained increasing attention in recent years and have become a common clinical chemistry procedure for the analysis of a wide range of analytes such as drugs, hormones, and proteins.[20] To the best of our knowledge, the use of CuInS$_2$/ZnS NCs as a fluorescence label for FIA has not been reported.

Interleukin 6 (IL-6) is a kind of cytokine that acts as both a proinflammatory and anti-inflammatory cytokine. Elevated levels of IL-6 are associated with clinical and subclinical cardiovascular disease.[21] The normal level of IL-6 in serum is in the range of 10−75 pg mL^{-1}, whereas individuals with various disease states have elevated IL-6 levels in the nanograms per milliliter.[22] High levels of IL-6 have also been correlated with prostate cancer in hormone-independent prostate cancer patients and breast cancer in AIDS patients.[23] Because of the importance of the biological and pathological functions of IL-6, it is highly desirable to develop rapid, sensitive, and specific method to determine the concentration of IL-6 for the reliable early detection of cancer and other diseases.

In this Article, we have developed a facile route for the synthesis of CuInS$_2$/ZnS NCs in an aqueous solution through microwave irradiation using GSH as a capping agent. The as-synthesized CuInS$_2$/ZnS NCs not only possess color-tunable properties ranging from the visible to the near-infrared (540−680 nm) but also long PL lifetimes (690 ns) and small particle sizes (∼3.3 nm). The CuInS$_2$/ZnS NCs have good biocompatibility for use as fluorescent probes in the live-cell labeling of HeLa cells. Furthermore, on the basis of fluorescent CuInS$_2$/ZnS NCs, a sensitive FIA platform was developed for the determination of human IL-6. The detailed experimental process is shown in Scheme 1. The results show that the CuInS$_2$/ZnS NCs are promising fluorescent labels for use in FIA for the detection of human IL-6.

Scheme 1. Schematic Illustration of the Fluoroimmunoassay for IL-6

Y Ab1   ● IL-6   Y Ab2-CuInS$_2$/ZnSNCs
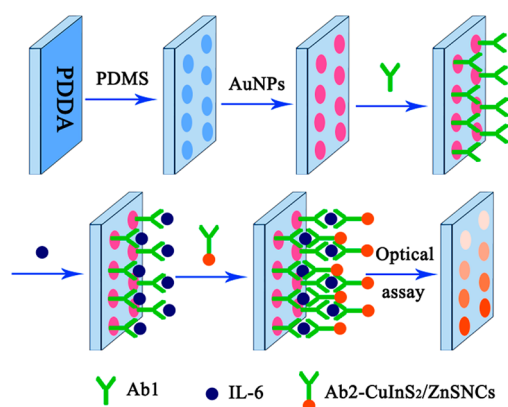
■ EXPERIMENTAL SECTION

Materials. Indium chloridehydrate (InCl$_3$·4H$_2$O, 99.9%) and reduced glutathione (GSH, 99%) were purchased from Aladdin Chemistry Co. Ltd. (China). Cupric nitrate (Cu(NO$_3$)$_2$, 99.5%), zinc acetate dehydrate (Zn(Ac)$_2$·2H$_2$O, 98%), and sodium sulfide (Na$_2$S, 99%) were purchased from Nanjing Chemical Reagent Co. Ltd. (China). Rhodamine 6G (99%), 1-ethyl-3-(3-dimethylaminopropyl) carbodiimide hydrochloride (EDC), bovine serum albumin (BSA), poly(diallyldimethylammonium chloride) (PDDA, 20%, w/w in water, MW 200 000−350 000), and Tween-20 were purchased from Sigmal-Aldrich. Human interleukin-6 (IL-6) as well as the capture (Ab$_1$) and

signal IL-6 antibodies (Ab$_2$) were purchased from Beijing Biosynthesis Biotechnology Co. Ltd. (China). All other reagents were of analytical reagent grade and used without further purification.

Microwave-Assisted Synthesis of CuInS$_2$/ZnS NCs. In a typical synthesis, 19.2 mL of an aqueous solution containing 0.01 mmol of Cu(NO$_3$)$_2$, 0.04 mmol of InCl$_3$, and 0.2 mmol of GSH was prepared in an exclusive vitreous vessel with a volume of 80 mL. The pH of the solution was adjusted to 8.5 by the addition of a 1.0 M NaOH solution. Under vigorous stirring, the solution changed from turbid to clear. Next, 0.8 mL of a freshly prepared Na$_2$S solution (0.05 M) was added into the mixture solution as the CuInS$_2$ precursor. High-quality CuInS$_2$ NCs were prepared at a controlled reaction temperature of 100 °C by CEM. After microwave irradiation for 5 min, the mixture was allowed to cool to lower than 50 °C. Then, 0.8 mL of 0.1 M Zn(Ac)$_2$ and 0.8 mL of 0.05 M Na$_2$S solutions were injected into the CuInS$_2$ NCs for the preparation of the CuInS$_2$/ZnS NCs. The mixture solution was further irradiated at 100 °C for 5 min, followed by purification using ultrafiltration with a Microcon YM-30 kDa filtration device.

Cellular MTT Assay and Confocal Fluorescence Imaging. HeLa cells were trypsinized and resuspended in Dulbecco's modified Eagle's medium (DMEM) supplemented with 10% fetal bovine serum and 1% penicillin/streptomycin. The cells (∼5 × 10^5 cells mL^{-1}) were seeded in a 96-well microplate in 100 μL of complete DMEM culture medium and were incubated at 37 °C in a humidified atmosphere with 5% CO$_2$ for 12 h. The DMEM was then replaced with fresh DMEM in the presence of different concentrations of CuInS$_2$/ZnS NCs or in the absence of CuInS$_2$/ZnS NCs (for blank experiments), and the cells were incubated for 24 h. One hundred microliters of the new culture media containing MTT (10 μL, 5 mg mL^{-1}) was added followed by incubation for 4 h to allow the formation of the formazan dye. The medium was then removed, and 110 μL of dimethyl sulfoxide (DMSO) was added to dissolve the purple formazan crystals followed by a 10 min incubation. Absorbance was measured at 490 nm in a Bio-Rad 680 microplate spectrophotometer. The relative cell viability was defined as (A_{test}/A_{blank}) × 100%, where A is the absorbance.

The confocal fluorescent images were taken with a Leica TCS SP5 inverted confocal microscope. First, HeLa cells were placed on a 35 mm petri dish with a 15 mm bottom well in DMEM with 10% fetal bovine serum in 5% CO$_2$ at 37 °C overnight to obtain a suitable cell density. Second, HeLa cells were pretreated with 0.05 mg mL^{-1} CuInS$_2$/ZnS NCs in serum-free DMEM for 2 h. The stained cells were carefully rinsed with PBS to remove the unbound CuInS$_2$/ZnS NCs before imaging.

Bioconjugation of CuInS$_2$/ZnS NCs with Antibodies. The conjugation procedure of CuInS$_2$/ZnS NCs with Ab$_2$ was similar to previous reports.[24,25] One hundred microliters of a freshly prepared EDC solution (4.2 mg mL^{-1}) was added to 1 mL of purified CuInS$_2$/ZnS NCs (dissolved in 10 mM PBS, pH 7.4), and the solution was vortexed for 20 min. Next, 400 μL of Ab$_2$ (0.1 mg mL^{-1}) was added to the mixture. The solution was incubated at room temperature and shaken in the dark for 24 h. The unreacted CuInS$_2$/ZnS NCs and the byproduct of the conjugation were removed by ultrafiltration using a 30 000 MW filter. After the lower phase was removed, the upper phase containing the CuInS$_2$/ZnS NCs-antibody conjugates was decanted and diluted to 0.5 mL with PBS followed by the addition of 0.5 mL of 10 mM PBS with 1% BSA. The solution was stored at 4 °C.

Preparation of the FIA. The FIA was performed on an object slide chip coated with a PDDA-AuNPs monolayer. Before modification, the chips were dipped into a solution of 1:1 (v/v) ethanol/NaOH (1 M) for 30 min after cleaning with acetone, ethanol, and water in sequence. The chips were rinsed with distilled water and dipped in a 0.05% PDDA aqueous solution for 30 min to modify them with a monolayer of PDDA. Then, the chips were rinsed with distilled water and dried under a stream of nitrogen, and a 2 mm thick poly(dimethylsiloxane) (PDMS) with a circular opening of 3 mm was bound to chip surface to form the specific reaction area. Twenty microliters of an AuNPs solution was added into the hole and was adsorbed on the substrate by electrostatic adsorption. Afterward, 20 μL of Ab$_1$ solution was spread onto the chip surface and incubated at 4 °C in a moist chamber for 12 h. After incubation, the chip was rinsed with PBST (PBS + 0.05% Tween-20) to remove physically
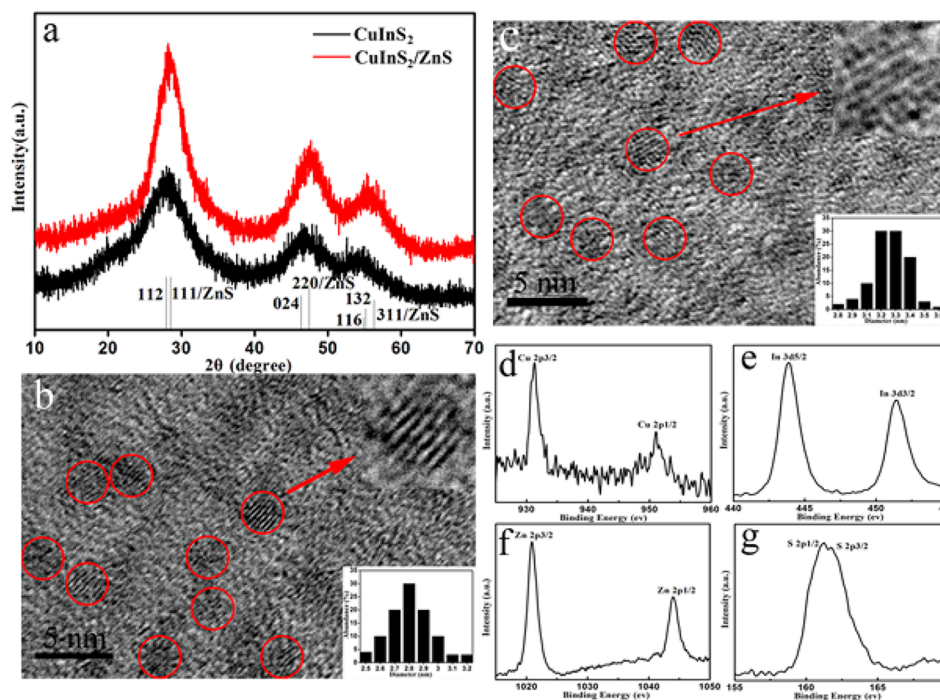
Figure 1. (a) X-ray diffraction patterns of the CuInS$_2$ NCs and CuInS$_2$/ZnS NCs. HRTEM images of (b) the CuInS$_2$ NCs and (c) CuInS$_2$/ZnS NCs. XPS spectra of the CuInS$_2$/ZnS NCs: (d) Cu2P, (e) In3d, (f) Zn2P, and (g) S2p.
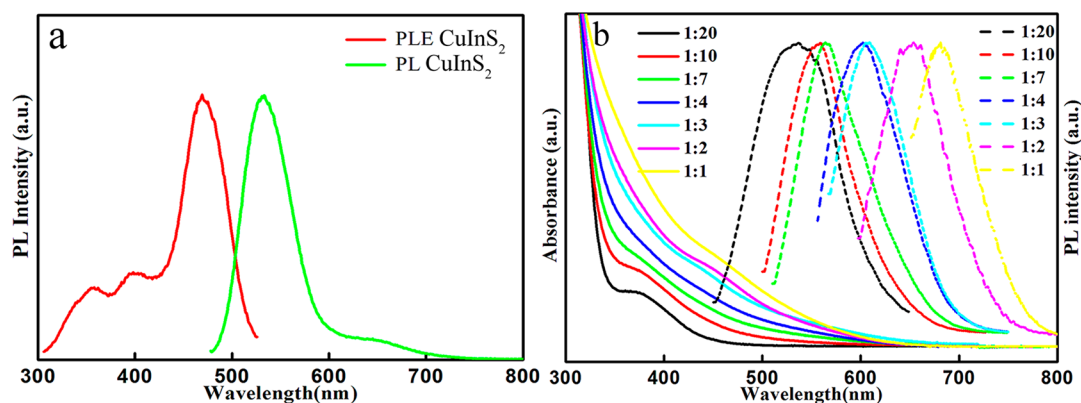

Figure 2. (a) PLE and PL spectra of the CuInS$_2$ NCs. (b) UV−vis absorption and PL spectra of the CuInS$_2$/ZnS NCs.

adsorbed Ab$_1$. The chip was then incubated in 2% BSA (in PBS) at 37 °C for 1 h to block excess active groups and nonspecific binding sites. The chip was washed with PBST and incubated with several different concentrations of human IL-6 (20 μL) at 37 °C for 50 min followed by washing with PBST to remove the nonspecific adsorption. Finally, 20 μL of CuInS$_2$/ZnS NCs-Ab$_2$ was added to the reaction area of the chip and incubated at 37 °C for another 50 min. To decrease the background response, the chip was washed with double-distilled water to remove nonspecifically bound CuInS$_2$/ZnS NCs-Ab$_2$. The entire experimental procedure is shown in Scheme 1.

Characterization. The UV−vis absorption and fluorescence spectra were obtained using a UV-3600 spectrophotometer and Bruker RF-5301PC fluorescence spectrometer, respectively. XRD patterns were obtained using XRD-6000 diffraction with Cu Kα radiation. X-ray photoelectron spectroscopy (XPS) was carried out on an ESCALAB MK II X-ray photoelectron spectrometer. High-resolution transmission electron microscopy (HRTEM) images were taken using a JEOL2010 electron microscope at an acceleration voltage of 200 kV. Fourier transform infrared (FTIR) spectra were recorded with a Bruker Vector 22 FTIR spectrometer. The confocal fluorescent images were taken with a Leica TCS SP5 inverted confocal microscope. The imaging software Quantity One is from Bio-Rad. Fluorescence microscopy images were

taken with a Nikon TE2000-U inverted optical microscope. The PL lifetime study was performed by FLS920 with an excitation of 409 nm. The microwave system is from Discover (CEM), and exclusive vitreous vessels with an 80 mL capacity were equipped for use with the system at high temperature and pressure.

■ RESULTS AND DISCUSSION

Structure Characterization. To evaluate the crystalline states and composition of the as-synthesized CuInS$_2$/ZnS NCs, XRD, HRTEM, XPS, and FTIR measurements were carried out. Figure 1a shows the XRD patterns of the CuInS$_2$ NCs and CuInS$_2$/ZnS NCs. The broad diffraction peaks suggest that they have small sizes. The XRD pattern of CuInS$_2$ NCs consists of three major peaks with 2θ values of 27.9, 46.3, and 54.8°, corresponding to the (112), (024), and (116) indices of the tetragonal crystal structure (CuInS$_2$, JCPDS no. 47-1372), respectively. The peaks positions of the CuInS$_2$/ZnS NCs was right shifted as compared to the XRD peaks of CuInS$_2$ NCs, suggesting that the crystal structure of the CuInS$_2$/ZnS NCs was slightly changed because of the diffusion of Zn^{2+}.[26] HRTEM was

8212

dx.doi.org/10.1021/am402328t | ACS Appl. Mater. Interfaces 2013, 5, 8210−8216

also used to characterize the crystalline structure and morphologies of the synthesized $CuInS_2/ZnS$ NCs. As shown in Figure 1b, the well-monodispersed $CuInS_2$ NCs showed average sizes of about 2.8 nm and displayed clear lattice fringes. After coating with a ZnS shell, the average size of the $CuInS_2/ZnS$ NCs increased to 3.3 nm (Figure 2c), indicating successful coating. The valence state of the $CuInS_2/ZnS$ NCs was characterized by the X-ray photoelectron spectrum. Figure 1d−f shows the high-resolution scans of Cu2p, In3d, Zn2p, and S2p photoelectron from $CuInS_2/ZnS$ NCs, respectively. The Cu2p core splits into $Cu2p_{3/2}$ (931.5 eV) and $Cu2p_{1/2}$ (951.2 eV) peaks, confirming that the valence states of Cu ions are +1 instead of +2, because the satellite peak at about 944.0 eV for Cu^{2+} only could not be observed.[27] Therefore, the results indicated that the oxidation state of Cu^{2+} was reduced by GSH during the reaction process. Moreover, the valences states of In^{3+} ($In3d_{5/2}$, 444.1 eV; $In3d_{3/2}$, 451.6 eV), Zn^{2+} ($Zn2p_{3/2}$, 1021.1 eV; $Zn2p_{1/2}$, 1044.2 eV), and S^{2-} ($S2p_{3/2}$, 161.4 eV) were also confirmed by XPS spectra (Figure 1, panels e, g, and f, respectively). The FTIR spectra of the pure GSH and GSH-capped NCs are compared in Figure S1 (Supporting Information). According to previous reports,[28] the IR absorption bands of free GSH at 3120 and 3014 cm^{-1} are ascribed to N−H stretching bands (NH_3^+), whereas the peaks at 2520 and 1538 cm^{-1} are assigned to −SH and −NHR groups, respectively. Comparing the IR spectrum of GSH-capped NCs with that of the pure GSH, the disappearance of the −SH stretching vibrational peak, the near disappearance of the N−H stretching bands, and the weakening of the amide bond clearly indicate that GSH may combine on the surface of the NCs through the −SH and −NHR groups.

UV−vis Absorption and PL spectra. The PL spectra and the PL excitation (PLE) spectra of the $CuInS_2$ NCs are shown in Figure 2a. The PL emission spectrum shows a peak at 530 nm accompanied by a weak broad shoulder peak at about 650 nm. The PLE spectrum spans from 300 to 550 nm. It is worth noting that tunable emissions are highly expected by varying the Cu/In molar ratios of the precursors. Unfortunately, the PL peak position of the $CuInS_2$ NCs remains at 530 nm without any change. The PL quantum yields (QYs) of the $CuInS_2$ NCs were about 1.5% with a Cu/In ratio of 1:4.

To improve the stability and PL properties, we prepared $CuInS_2$-based core/shell NCs by coating with a ZnS shell layer. Figure 2b shows the UV−vis absorption and PL spectra of the $CuInS_2/ZnS$ NCs with different Cu/In molar ratios. The UV−vis absorption spectrum (solid line) of $CuInS_2/ZnS$ NCs shows broad absorption spectra without distinct excitonic absorption features. This is consistent with previous reports for I−III−VI semiconductor nanocrystals.[12] With increasing Cu/In ratios of the precursor from 1:20 to 1:1 (the exact components of the Cu/In ratios measured by EDS and ICP are shown in Table S1, Supporting Information), the absorption onset wavelength was gradually red shifted from ca. 470 to 640 nm. Besides, the red shift was also observed in the emission peak of the $CuInS_2/ZnS$ NCs (from 540 to 680 nm) with the change in the increment of the Cu/In molar ratios. This tendency was in good agreement with that of the absorption onset shown in the UV−vis absorption spectra. The photographs of water-soluble $CuInS_2/ZnS$ NCs under 365 nm UV illumination are shown in Figure 3. Furthermore, a large Stokes shift and broad emission peaks with a full-width at half-maximum (fwhm) of larger than 110 nm were observed. These indicate that the PL was not band-edge emission

Figure 3. Digital photographs of the $CuInS_2/ZnS$ NCs under excitation at 365 nm UV (3:4, 1:2, 3:8, 1:3, 1:4, 1:5, and 1:10).

but was assigned to the radiative transition in the donor−acceptor level or the emission from trap sites.[29]

To understand better the PL mechanism of the $CuInS_2/ZnS$ NCs, the PLE peaks of $CuInS_2/ZnS$ NCs with different Cu/In ratios are shown in Figure 4a. The $CuInS_2/ZnS$ NCs have two main excitation peaks that are dependent on the Cu/In ratios. With the increasing ratio of Cu/In from 1:20 to 1:2, the peak at around 380 nm becomes weakened gradually, whereas the other peak is red shifted from around 450 to 590 nm. Figure 4b shows the relationship between the PL QYs and the chemical composition of the $CuInS_2/ZnS$ NCs. The optimal PL QYs of ca. 24% was obtained for $CuInS_2/ZnS$ NCs with Cu/In of 1:4, and either a decrease or an increase of the Cu content in the NCs simply decreases the PL QYs. It has been reported that the PL of I−III−VI NCs originated from a donor−acceptor transition mechanism, where In_{Cu} (In substituted at the Cu site) and/or V_S (S vacancy) are likely to act as donor states and V_{Cu} (Cu vacancy), as an acceptor state.[12,30] An alternative carrier recombination between the quantized conduction band minimum and defect (acceptor) trap level is also persuasive as proposed by Nose et al.[31] The amount of Cu vacancies has been reported to play an important role in the enhancement of PL intensity, and the PL intensity increased with Cu/In ratios.[30] On one hand, the appropriate In/Cu ratio can help carrier recombination, enhancing the fluorescence. On the other hand, when the In/Cu ratios were large enough, the concentration of the recombination center increased dramatically, suppressing the PL emission.

Influence of GSH Concentration and pH Value on the Optical Properties of the $CuInS_2/ZnS$ NCs. To study the PL properties of $CuInS_2/ZnS$ NCs, we investigated the effect of the In/GSH ratios and pH value on the PL intensity. In Figure 5a, it can be seen that the molar ratios of In/GSH greatly affected the PL intensity of the as-prepared $CuInS_2/ZnS$ NCs. The PL intensity reached the maximum when the ratio of In/GSH was 1:5. Meanwhile, the pH value also plays an important role in the PL intensity of $CuInS_2/ZnS$ NCs, as shown in Figure 5b. The pH value changed from 8 to 11. When the pH value was below 8, the solution turned turbid. When the pH value was 8, the PL intensity reached the maximum. In addition, we investigated the fluorescence intensity and photostability of the as-prepared $CuInS_2/ZnS$ NCs at different pH values and irradiation, as shown in Figures S2 and S3, respectively. (Supporting Information)

PL Lifetimes. Figure 6 and Table 1 show the PL decay curves and the corresponding PL lifetimes of the $CuInS_2$ NCs and $CuInS_2/ZnS$ NCs with different Cu/In ratios, respectively. The decay curves were multiexponential in nature and were excited at 409 nm. The decay curves were fitted well by the following equation
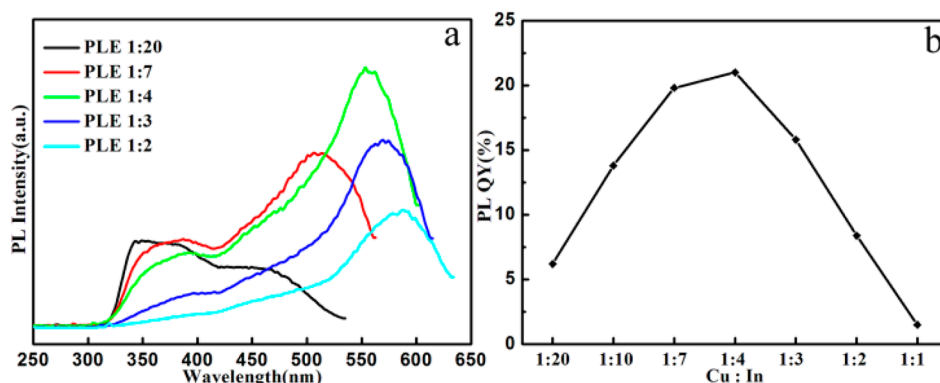

Figure 4. (a) PLE spectra of the CuInS$_2$/ZnS NCs. (b) Relationship between the PL QYs and the chemical composition of the CuInS$_2$/ZnS NCs.
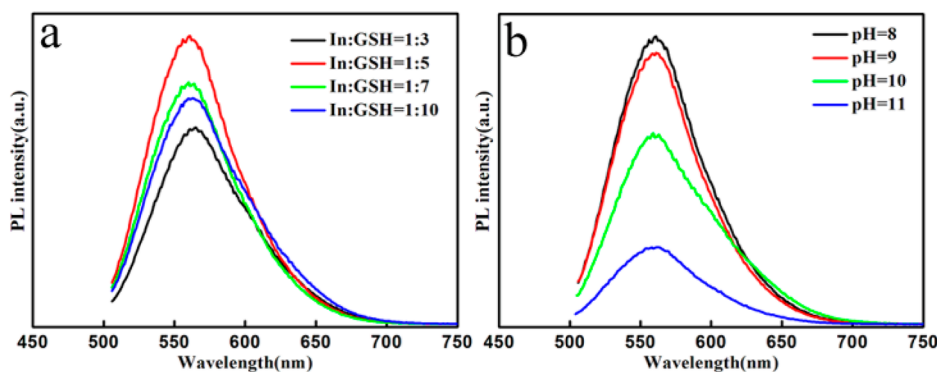

Figure 5. PL intensity of the CuInS$_2$/ZnS NCs with different (a) ratios of In/GSH and (b) pH value.
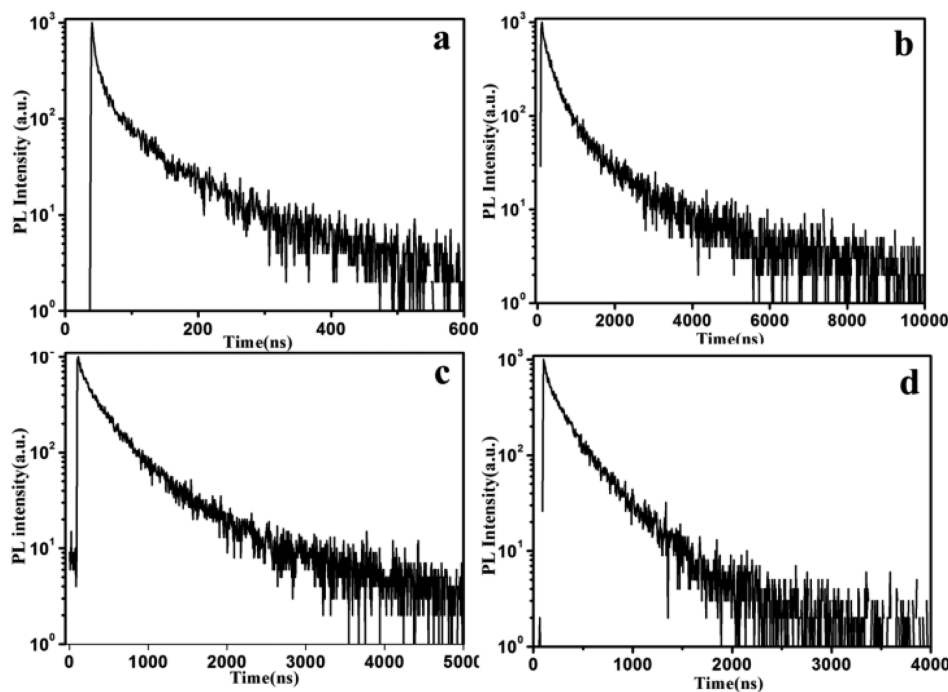

Figure 6. PL decays curves of the CuInS$_2$ NCs and CuInS$_2$/ZnS NCs with different Cu/In ratios.

$$I(t) = A_1 \exp\left(-\frac{t}{\tau_1}\right) + A_2 \exp\left(-\frac{t}{\tau_2}\right)$$

where τ_1 and τ_2 represent the decay time of the PL mission and A_1 and A_2 represent the relative weights of the decay components at $t = 0$. On the basis of the obtained lifetime values in Table 1, we

attribute the fast decay time (τ_2) component to the radiative recombination processes of the surface defect states, whereas the slower decay time (τ_1) is due to the radiative recombination processes of the donor−acceptor pairs or the deep defect-related recombination mechanism. Surface-related trap states are usually shallow and therefore show a faster decay lifetime compared to

Table 1. Double-Exponential Fitting Results for PL Decay Profiles of NCs Prepared from Precursors with Different Cu/In Ratios

sample	Cu/In	τ_1 (ns)	A_1 (%)	τ_2 (ns)	A_2 (%)	lifetime (ns)
a	CuInS$_2$ NCs (1:5)	94.3	68.9	14.5	31.1	68.4
b	CuInS$_2$/ZnS NCs(1:10)	1155.3	48.8	247	51.2	690.3
c	CuInS$_2$/ZnS NCs(1:5)	720.5	55.61	211.2	44.39	494.5
d	CuInS$_2$/ZnS NCs(3:8)	378	69.7	100	30.4	293.9

the intrinsic defect-related trap states.[32,33] The average lifetime of the CuInS$_2$ NCs without the ZnS shell layers (68.4 ns, Cu/In 1:5) is significantly shorter than that with the ZnS shell layers (494.5 ns). This indicated that with the coating of the ZnS layer, some of the surface-related nonradiative carrier losses have been eliminated by the ZnS layer.

MTT and Cell Imaging. To show their potential use in a bioapplication, the CuInS$_2$/ZnS NCs were incubated directly with HeLa cells. The fluorescence images of HeLa cells were taken with a Leica TCS SP5 inverted confocal microscope, as shown in Figure S4 (Supporting Information). A strong fluorescence emission from the CuInS$_2$/ZnS NCs in the HeLa cells can be observed, indicating that the CuInS$_2$/ZnS NCs successfully enter into the HeLa cells. Furthermore, MTT assays were carried out to evaluate the cytotoxicity of the CuInS$_2$ NCs and CuInS$_2$/ZnS NCs on the HeLa cells. As expected, the viability of the HeLa cells declined by only <5% upon the addition of the CuInS$_2$/ZnS NCs at concentrations of up to 0.20 mg mL^{-1} (Figure S5). Thus, the as-prepared CuInS$_2$/ZnS NCs can be considered to be low in toxicity and biocompatible for cell fluorescence imaging.

Fluoroimmunoassay Analysis of IL-6. Because of the attractive properties of CuInS$_2$/ZnS NCs, such as their low toxicity, high fluorescence, and good biocompatibility, the CuInS$_2$/ZnS NCs can be used as the signal labels for the FIA analysis of the biomarker IL-6. Scheme 1 shows the illustration of the sandwich FIA on the microarray format with a PDDA-AuNPs-modified object slide chip. The primary antibody, anti-IL-6, was printed on the chip and immobilized on the surface through electrostatic interactions and the Au–S bond. The antibody-modified chip was blocked with 2% skim milk to reduce

the nonspecific binding. After washing with PBST, the primary antibody-immobilized chip was incubated with antigen (IL-6) to form the complex. Following routine washing, the chip was incubated with a secondary anti-IL-6 antibody conjugated with CuInS$_2$/ZnS NCs to form sandwich-type immunocomplexes. The fluorescence image and fluorescence intensity of the chip was analyzed with an inverted fluorescence microscope and the imaging software Quantity One, respectively. Figure 7a–g shows the fluorescence image of the immunochip with different concentrations of IL-6. It can be observed that the intensity of the fluorescence images decreases with the decreasing antigen concentration from 2 μg mL^{-1} to 0.02 ng mL^{-1}. The resulting calibration curve (Figure 7h) of the fluorescence intensity versus IL-6 concentration plotted on a semilog scale is linear from 0.02 ng mL^{-1} to 20 ng mL^{-1}. The detection limit is 0.008 ng mL^{-1}. The controls sample without the presence of IL-6 showed almost no fluorescence.

The feasibility of the FIA for clinical applications was investigated by analyzing real samples in comparison with the ELISA method. These serum samples were diluted with PBS (pH 7.4). The comparison is shown in Table S2 (Supporting Information). The relative deviation of these methods is from −4.5 to 10.6%, suggesting that there is no significant difference between our method and the ELISA. Specificity is an important criterion for the FIA. The potential interference for IL-6 detection from coexisting species such as TNF-α and IgG was studied with the FIA. The resulting fluorescence images show that the signal from the nonspecific test protein was negligible. Furthermore, the chip has no obviously significant change after being stored in a refrigerator at 4 °C for 1 month.

■ CONCLUSIONS

Low-toxicity, color-tunable, water-soluble CuInS$_2$/ZnS NCs have been rapidly synthesized via a microwave-assisted approach. The as-prepared CuInS$_2$/ZnS NCs are high quality and have tunable emission properties in the wavelength range from 540 to 680 nm by varying the initial amount of the In/Cu ratio in the precursors. The as-prepared CuInS$_2$/ZnS NCs have good biocompatibility and longer average lifetimes than the Cd-based NCs. Furthermore, the CuInS$_2$/ZnS NCs were used as the signal labels for the FIA analysis of the biomarker IL-6, showing their potential for use as biomarker signal probes in diagnostic applications for cancer and other diseases.
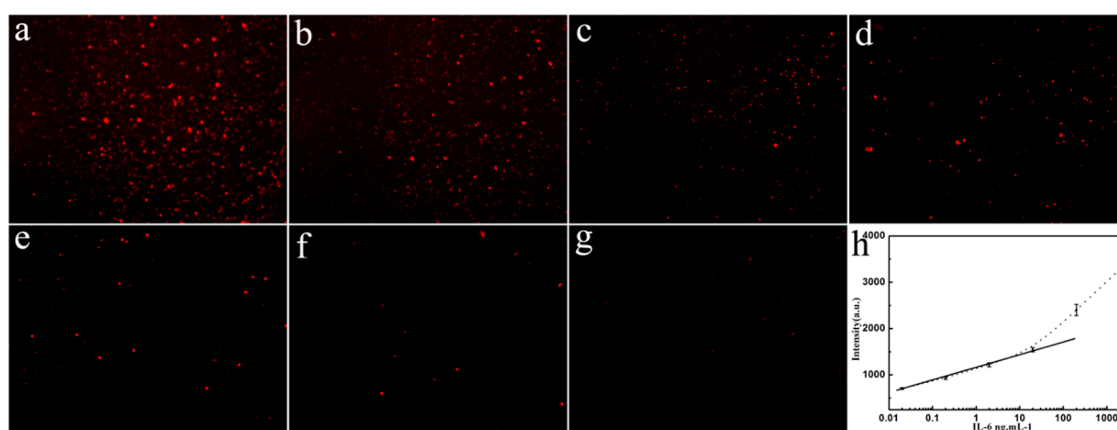

Figure 7. Fluorescence images of IL-6 on the chip with different concentrations antigen (a–g: 2000, 200, 20, 2, 0.2, 0.02, and 0 ng mL^{-1}, respectively). (h) Resulting calibration curve of IL-6 plotted on a semilog scale.

■ ASSOCIATED CONTENT

ⓢ Supporting Information
FTIR spectra of glutathione and $CuInS_2/ZnS$ NCs, fluorescence intensity of the $CuInS_2/ZnS$ NCs at different pH values, photostability of the $CuInS_2/ZnS$ NCs, bright-field and fluorescence images of HeLa cells incubated with $CuInS_2/ZnS$ NCs, viability of HeLa cells incubated with $CuInS_2$ NCs and $CuInS_2/ZnS$ NCs, atom ratios of $CuInS_2$ NCs measured by EDS and ICP, and human serum IL-6 levels determined using FIA and ELISA. This material is available free of charge via the Internet at http://pubs.acs.org.

■ AUTHOR INFORMATION

Corresponding Author
*Tel/Fax: +86 25 83597204. E-mail: wuxingca@nju.edu.cn (X.-C.W.), jjzhu@nju.edu.cn (J.-J.Z.).
Notes
The authors declare no competing financial interest.

■ ACKNOWLEDGMENTS

■ REFERENCES

(1) Du, Y. P.; Xu, B.; Fu, T.; Cai, M.; Li, F.; Zhang, Y.; Wang, Q. B. *J. Am. Chem. Soc.* **2010**, *132*, 1470.
(2) Gu, Y. P.; Cui, R.; Zhang, Z. L.; Xie, Z. X.; Pang, D. W. *J. Am. Chem. Soc.* **2011**, *134*, 79.
(3) Mao, B. D.; Chuang, C. H.; Lu, F.; Sang, L. X.; Zhu, J. J.; Burda, C. *J. Phys. Chem. C.* **2013**, *117*, 648.
(4) Choi, H. S.; Liu, W. H.; Misra, P.; Tanaka, E.; Zimmer, J. P.; Ipe, B. I.; Bawendi, M. G.; Frangioni, J. V. *Nat. Biotechnol.* **2007**, *25*, 1165.
(5) Mandal, G.; Darragh, M.; Wang, Y. A.; Heyes, C. D. *Chem. Commun.* **2013**, *49*, 624.
(6) Cheng, F. F.; Liang, G. X.; Shen, Y. Y.; Rana, R. K.; Zhu, J. J. *Analyst* **2013**, *138*, 666.
(7) Zhang, W. J.; Zhang, H.; Feng, Y. Y.; Zhong, X. H. *ACS Nano* **2012**, *6*, 11066.
(8) Zimmer, J. P.; Kim, S. W.; Ohnishi, S.; Tanaka, E.; Frangioni, J. V.; Bawendi, M. G. *J. Am. Chem. Soc.* **2006**, *128*, 2526.
(9) Hines, M. A.; Scholes, G. D. *Adv. Mater.* **2003**, *15*, 1884.
(10) Xie, R. G.; Rutherford, M.; Peng, X. G. *J. Am. Chem. Soc.* **2009**, *131*, 5691.
(11) Park, J.; Kim, S. W. *J. Mater. Chem.* **2011**, *21*, 3745.
(12) Nam, D. E.; Song, W. S.; Yang, H. *J. Mater. Chem.* **2011**, *21*, 18220.
(13) Liu, S. Y.; Zhang, H.; Qiao, Y.; Su, X. G. *RSC Adv.* **2012**, *2*, 819.
(14) Wang, M. N.; Liu, X. Y.; Cao, C. B.; Shi, C. *RSC Adv.* **2012**, *2*, 2666.
(15) Zhan, H. J.; Zhou, P. J.; He, Z. Y.; Tian, Y. *Eur. J. Inorg. Chem.* **2012**, *15*, 2487.
(16) Qian, H. F.; Qiu, X.; Li, L.; Ren, J. C. *J. Phys. Chem. B.* **2006**, *110*, 13352.
(17) Shen, Y. Y.; Li, L. L.; Lu, Q.; Ji, J.; Fei, R.; Zhang, J. R.; Abdel-Halim, E. S.; Zhu, J. J. *Chem. Commun.* **2012**, *48*, 2222.
(18) Xiong, W. W.; Yang, G. H.; Wu, X. C.; Zhu, J. J. *J. Mater. Chem. B.* **2013**, *1*, 4160.
(19) Pons, T.; Pic, E.; Lequeux, N.; Cassette, E.; Bezdetnaya, L.; Guillemin, F.; Marchal, F.; Dubertret, B. *ACS Nano* **2010**, *4*, 2531.
(20) Nichkova, M.; Feng, J.; Sanchez-Baeza, F.; Marco, M. P.; Hammock, B. D.; Kennedy, I. M. *Anal. Chem.* **2003**, *75*, 83.
(21) Wu, H.; Huo, Q. S.; Varnum, S. S.; Wang, J.; Liu, G. D.; Nie, Z. M.; Liu, J.; Lin, Y. H. *Analyst* **2008**, *133*, 1550.
(22) Peng, J.; Feng, L. N.; Ren, Z. J.; Jiang, L. P.; Zhu, J. J. *Small* **2011**, *7*, 2921.
(23) Moosmayer, D.; Berndorff, D.; Chang, C. H.; Sharkey, R. M.; Rother, A.; Borkowski, S.; Rossi, E. A.; McBride, W. J.; Cardillo, T. M.; Goldenberg, D. M.; Dinkelborg, L. M. *Clin. Cancer Res.* **2006**, *12*, 5587.
(24) Cui, R.; Pan, H. C.; Zhu, J. J.; Chen, H. Y. *Anal. Chem.* **2007**, *79*, 8494.
(25) Liu, H. Y.; Wu, X. M.; Zhang, X.; Burda, C.; Zhu, J. J. *J. Phys. Chem. C.* **2012**, *116*, 2548.
(26) Tang, X. S.; Ho, W. B. A.; Xue, J. M. *J. Phys. Chem. C.* **2012**, *116*, 9769.
(27) Peng, S. J.; Liang, Y. L.; Cheng, F. Y.; Liang, J. *Sci. China: Chem.* **2012**, *55*, 1236.
(28) Wang, Q. S.; Fang, T. T.; Liu, P.; Deng, B. H.; Min, X. M.; Li, X. *Inorg. Chem.* **2012**, *51*, 9208.
(29) Chang, J. Y.; Wang, G. Q.; Cheng, C. Y.; Lin, W. X.; Hsu, J. C. *J. Mater. Chem.* **2012**, *22*, 10609.
(30) Song, W. S.; Yang, H. *Chem. Mater.* **2012**, *24*, 1961.
(31) Nose, K.; Soma, Y.; Omata, T.; Otsuka-Yao-Matsuo, S. *Chem. Mater.* **2009**, *21*, 2607.
(32) Li, L.; Pandey, A.; Werder, D. J.; Khanal, B. P.; Pietryga, J. M.; Klimov, V. I. *J. Am. Chem. Soc.* **2011**, *133*, 1176.
(33) Komarala, V. K.; Xie, C.; Wang, Y. Q.; Xu, J.; Xiao, M. *J. Appl. Phys.* **2012**, *111*, 124314.